Table S1. Previous studies on precipitation using the MRI-AGCM3

Study	Model version[a]	Cumulus convection scheme[b]	Period	Future emission scenario[c]	Future sea surface temperature (SST)[d]	Region	Results
Kusunoki et al. (2006)	3.0S	AS	around 1990, 10 years around 2090, 10 years	SRES A1B	MRI-CGCM2.3.2	East Asia	Precipitation and its intensity increase in rainy season. Termination of rainy season delays over Japan.
Kitoh and Kusunoki (2007)	3.0S, L	AS	1979-1998, 20 years			Asia	The 20-km model performs better than the 180-km model in simjulating precipitation.
Kusunoki and Mizuta (2008)	3.0S	AS	1979-1998, 20 years 2080-2099, 20 years	SRES A1B	MRI-CGCM2.3.2 MIROC3.2(hires)	East Asia	Precipitation and its intensity increase in rainy season. Termination of rainy season delays over Japan.
Kusunoki et al. (2011)	3.1S, H, L	AS	1979-2003, 25 years 2075-2090, 25 years	SRES A1B	CMIP3 MME mean MRI-CGCM2.3.2 MIROC3.2(hires) CSIRO-MK3.0	East Asia	Precipitation and its intencity increase in rainy season. Termination of rainy season delays. Projections by the 20-km model and 60-km models are consistent.
Kusunoki and Mizuta (2012)	3.1S, H	AS	1979-2003, 25 years 2015-2039, 25 years 2075-2090, 25 years	SRES A1B	CMIP3 MME mean MRI-CGCM2.3.2 MIROC3.2(hires) CSIRO-MK3.0	East Asia	The near future climate is located approximately midway between the present-day climate and the future climate.
Endo et al. (2012)	3.2S, H	YS, AS, KF	1979-2003, 25 years 2075-2099, 25 years	SRES A1B	CMIP3 MME mean three clusters	Asia	Precipitation and its intensity increase. Sensitivity of changs to cumulus convection and SSTs depends on region.
Kusunoki and Mizuta (2013)	3.2H	YS	1872-2099, 134 years	SRES A1B	CMIP3 MME mean	East Asia	Annual precipitation and precipitation intensity increases monotonically through the 21st century.
Kusunoki et al. (2015)	3.2H	YS	1872-2099, 134 years	SRES A1B	CMIP3 MME mean	Arctic	Annual precipitation and precipitation intensity increases monotonically through the 21st century.
Kusunoki (2016)	3.2S, H, L	YS, AS, KF	2081-2000, 20 years			East Asia	The MRI-AGCM3.2 performs better than CMIP5 model in simulating precipitation.

Table S1. Continued

Study	Model version[a]	Cumulus convection scheme[b]	Period	Future emission scenario[c]	Future sea surface temperature (SST)[d]	Region	Results
Kitoh and Endo (2016)	3.2S	YS	2079-2003, 25 years 2075-2099, 25 years	RCP8.5	CMIP5 MME three clusters	Global	Heavy precipitation increases in globally, evenwhere mean precipitation decrease.
Mizuta et al. (2017)	3.2H	YS	1951−2010, 60 years 100 member ensemble around 2090, 60 years 90 member ensemble	RCP8.5	CCSM4, GFDLCM3, HadGEM2-AO, MIROC5, MPI-ESM-MR, MRI-CGCM3	Global	Probabilistic future changes in extreme events are available directly without using any statistical models.
Endo et al. (2017)	3.2H	YS	1951−2010, 60 years 100 member ensemble around 2090, 60 years 90 member ensemble	RCP8.5	CCSM4, GFDLCM3, HadGEM2-AO, MIROC5, MPI-ESM-MR, MRI-CGCM3	East Asia	Heavy precipitation increases. Uncertainty of SST pattern affects uncertainty of precipitation change over oceans.
Kusunoki (2017)	3.2H	YS, AS, KF	2083-2003, 21 years 2079-2099, 21 years	RCP8.5	CMIP5 MME mean three clusters	East Asia	Precipitation intensity increases. Onset of rainy season delays over Japan.
This study	3.2S, H, L	YS, AS, KF	2083-2003, 21 years 2079-2099, 21 years	RCP8.5	CMIP5 MME mean three clusters	Global	Conversion rate of precipitation from water vapor by heavy precipitation is larger than that by moderate and weak precipitation.

[a] Grid size: S=20 km, H=60 km, L=180 km

[b] YS=Yoshiumura, Yoshimura et al. (2015)
AS=Arakawa-Schubert, Randal and Pan (1993)
KF=Kain-Fritsch, Kain and Fritsch (1990)

[c] SRES: Special Report on Emission Sccenario, IPCC (2000)
RCP: Representative Concentration Pathway, Collins et al. (2013)

[d] CMIP3: The third phase of the Coupled Model Intercomparison Project
CMIP5: The fifith phase of the Coupled Model Intercomparison Project
MME: Muti-Model Ensemble

Table S2. Features of 24 CMIP5 models used in this study. Target period; 1983-2003, 21 years. Three versions of MRI-AGCM with different horizontal resolution are also listed for comparison; S=20 km, H=60 km, L=180 km.

No.	Name in Table 9.A.1 of IPCC (2013)	Horizontal resolution and vertial levels[a]	Number of grids		Longitudinal grid spacing (km) at 35 ºN
			Longitude	Latitude	
1	ACCESS1.0	G63L17	192	145	171
2	ACCESS1.3	G63L17	192	145	171
3	BCC-CSM1.1	T42L17	128	64	256
4	BCC-CSM1.1(m)	T106L17	320	160	102
5	BNU-ESM	T42L17	128	64	256
6	CanAM4	T42L22	128	64	256
7	CCSM4	T95L17	288	192	114
8	CMCC-CM	T160L17	480	240	68
9	CNRM-CM5	T85L17	256	128	128
10	CSIRO-Mk3.6.0	T63L18	192	96	171
11	EC-EARTH	T106L16	320	160	102
12	FGOALS-g2	T42L17	128	60	256
13	GFDL-CM3	G47L23	144	90	228
14	GFDL-HIRAM-C180	G192L17	576	360	57
15	GFDL-HIRAM-C360	G384L17	1152	720	28
16	INM-CM4	G59L17	180	120	182
17	IPSL-CM5A-LR	T31L17	96	96	342
18	IPSL-CM5A-MR	T47L17	144	143	228
19	IPSL-CM5B-LR	T31L17	96	96	342
20	MIROC5	T85L17	256	128	128
21	MPI-ESM-LR	T63L25	192	96	171
22	MPI-ESM-MR	T63L25	192	96	171
23	MRI-CGCM3	T106L23	320	160	102
24	NorESM1-M	T47L17	144	96	228
	MRI-AGCM3.2S	T639L60	1920	960	17
	MRI-AGCM3.2H	T213L60	640	320	57
	MRI-AGCM3.2L	T63L60	192	96	171

[a] G denotes grid model. Two digits after G show corresponding spectral wave number.
The digits after T denotes the triangular runcation at the corresponding spectral wavenumber.
Two digits after L show vertical levels.

CMIP5: The fifith phase of the Coupled Model Intercomparison Project

8 IPCC: Intergovermental Panel of Climate Change

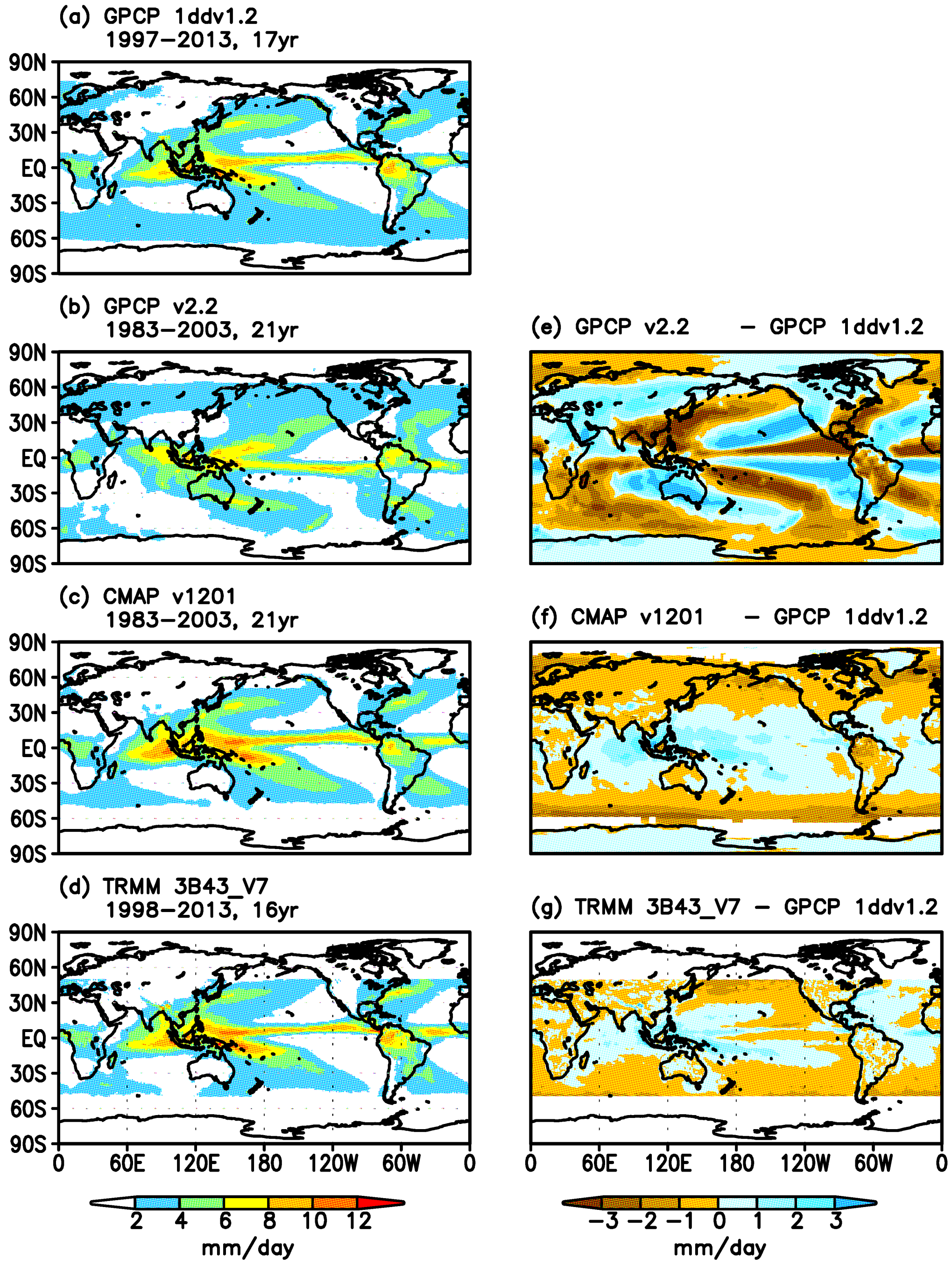

Figure S1. Comparison among observations for annual average precipitation (mm day^{-1}). (a) GPCP 1ddv1.2, 1.0 degree, 1997-2013, 17 years, (b) GPCP v2.2, 2.5 degree, 1983-2003, 21 years, (c) CMAP v1202, 2.5 degree, 1983-2003, 21 years, (d) TRMM 3B43 V7, 0.25 degree, 1998-2013, 16 years, (e) GPCP v2.2 - GPCP 1ddv1.2, (f) CMAP - GPCP 1ddv1.2, (f) TRMM - GPCP 1ddv1.2.

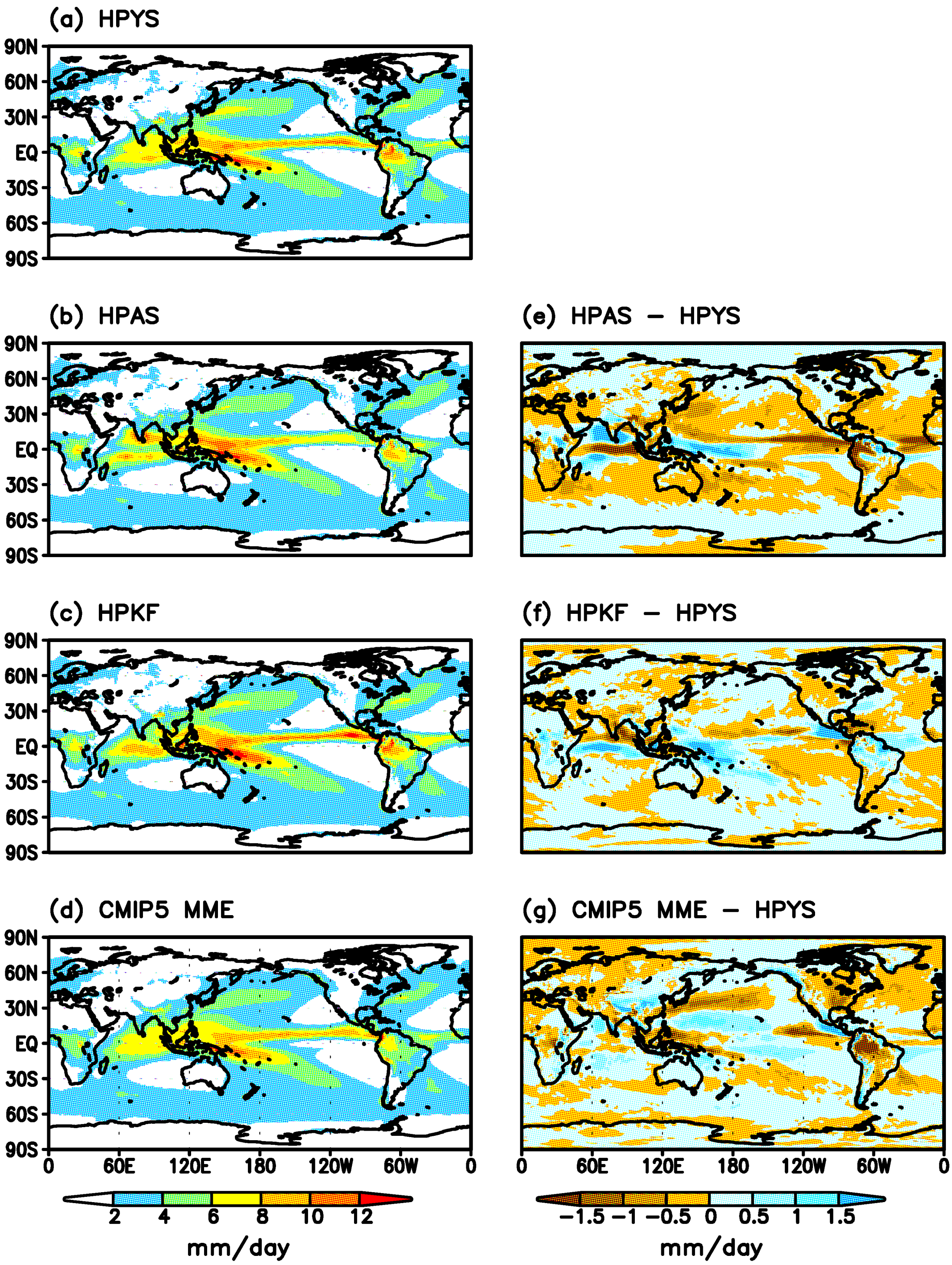

Figure S2. Comparison among simulations for annual average precipitation (mm day^{-1}). 1983-2003, 21 years. (a) HPYS, (b) HPAS, (c) HPKF, (d) CMIP5 MME mean, (e) HPAS - HPYS, (f) HPKF - HPYS, (g) CMIP5 MME mean - HPYS.

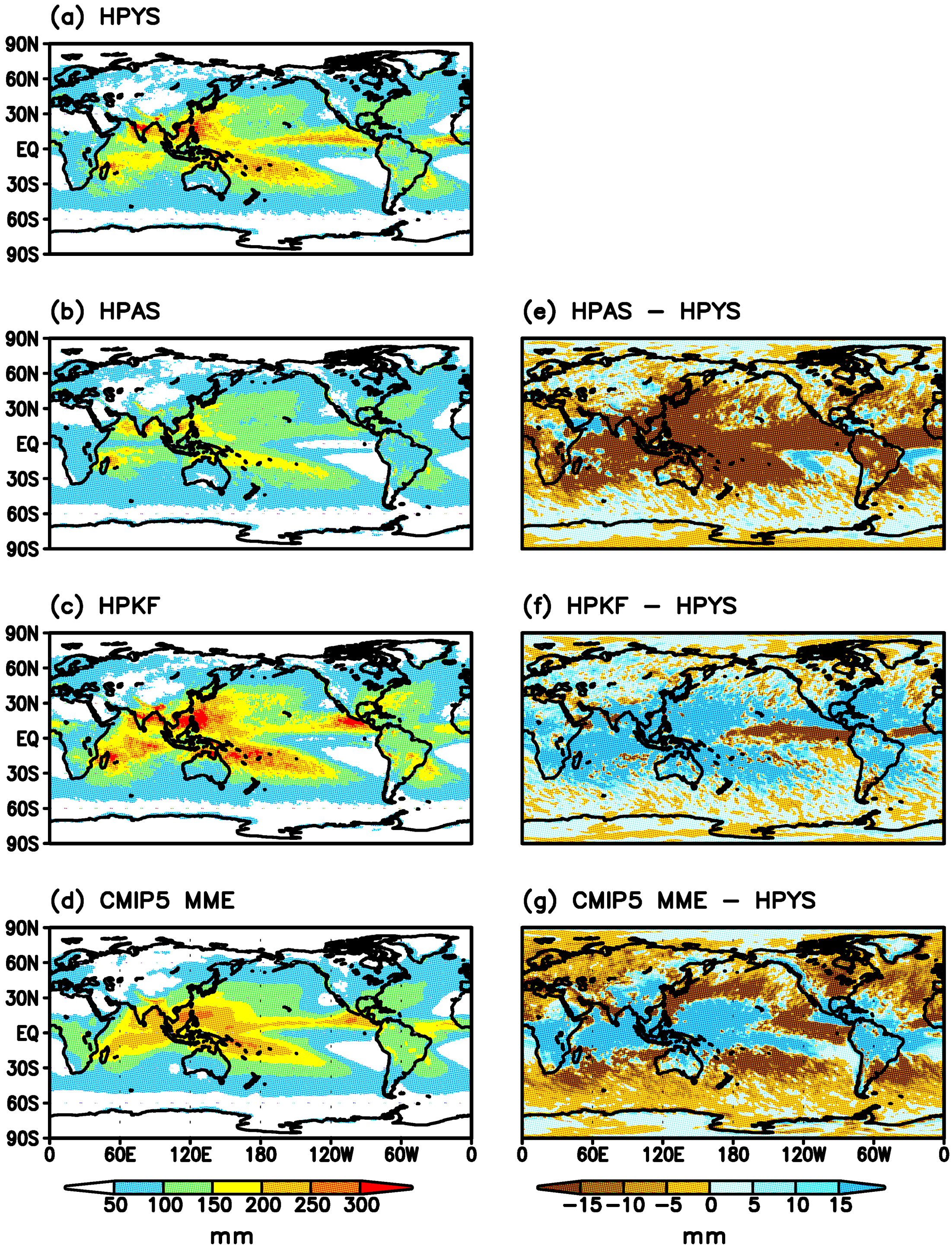

Figure S3. Same as Figure S2 but for R5d. Unit is mm.

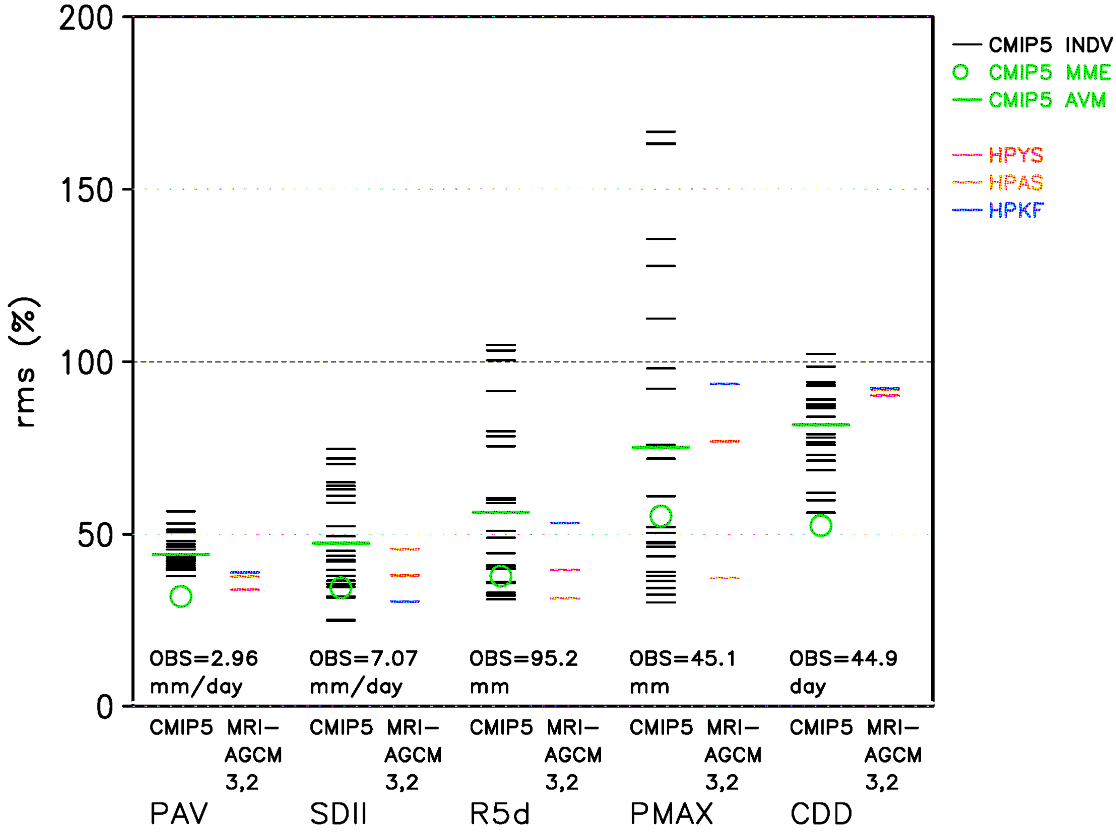

Figure S4. Root mean square errors (RMSE, %) of global distribution of precipitation indices (Table 3) between observations by GPCP 1ddv1.2 and model simulations. RMSEs are normalized by observed global averages indicated in the bottom of panel, respectively. Red, orange and blue bars denote the 60-km models with the YS, AS and KF schemes, respectively. Black bars show the CMIP5 individual models. Green circles indicate the MME of CMIP5 models. Green bars indicate the AVM of CMIP5 models.

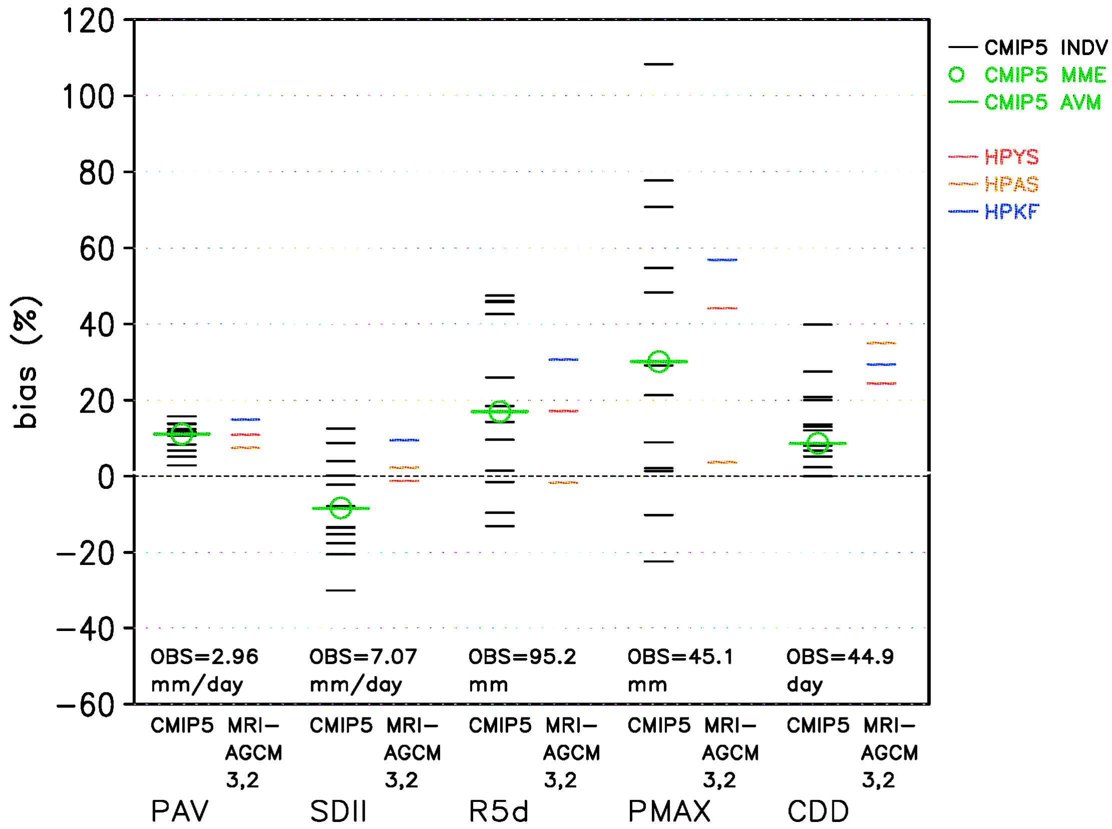

Figure S5. Same as figure S2 but for bias.

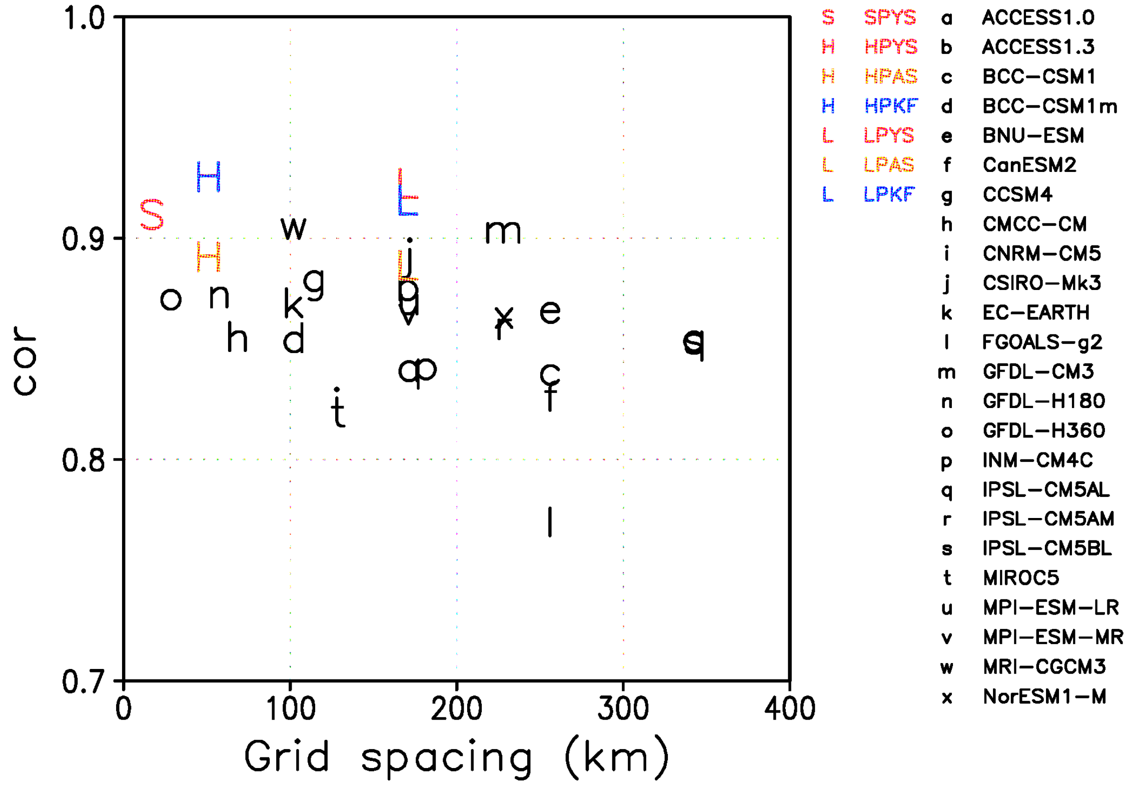

Figure S6. Dependence of model skill on the grid spacing (35°N) of 31 models including 7 MRI-AGCM3.2 models (color) and 24 CMIP5 (black) atmospheric models. The skill measure is the spetial correlation coefficient *R* between the GPCP 1DD observations and simulations over the globe for annual mean precipitation PAV. The correlation coefficient between grid spacing and *R* is -0.410, which exceeds the 95% significance level based on Student's t test. Grid spacing of models are given in the last column of Table S1. Letter S, H, L denote MRI-AGCM3.2S, MRI-AGCM3.2H, MRI-AGCM3.2L, respectively (Table S2). Red, orange, blue colors denote the YS, AS, KF schemes, respectively. For the MRI-AGCM3.2 models, only the first member of ensemble simulations is selected in order to exclude excessive and unfair contribution of specific models. Note that red H is overlapped and hidden by blue H.

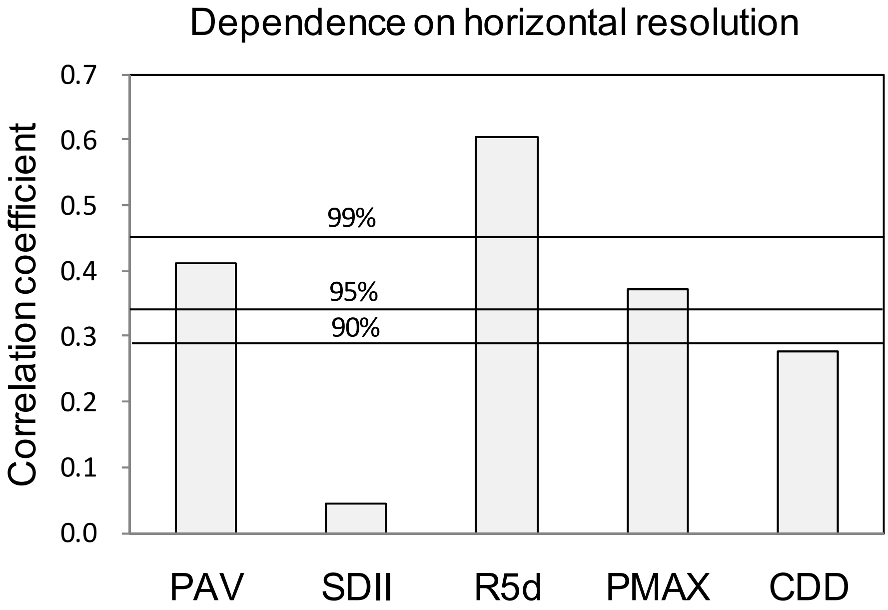

Figure S7. Correlation coefficients between the skill and grid size of 31 models including 7 MRI-AGCM3.2 models and 24 CMIP5 atmospheric models (Table S1) over the globe with respect to PAV and 4 extreme indices. The MRI-AGCM3.2 models include SPYS, HPYS, HPAS, HPKF, LPYS, LPAS and LPKF. The skill is based on the spatial correlation coefficient *R* (sign is reversed) between the GPCP 1DD observation and simulation over the globe. Horizontal lines show statistical significance levels. Scatter plot in the case of PAV is displayed in Figure S6.

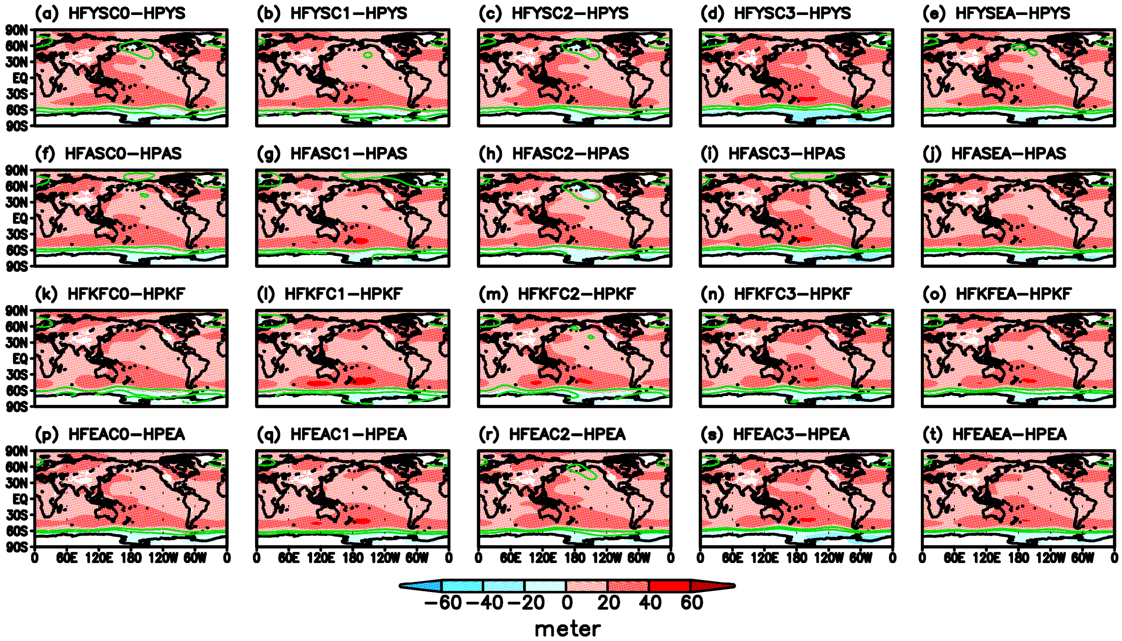

Figure S8. Same as Figure 5 but for 850 hPa height (meter). Green contour denotes the 95 % significance level.

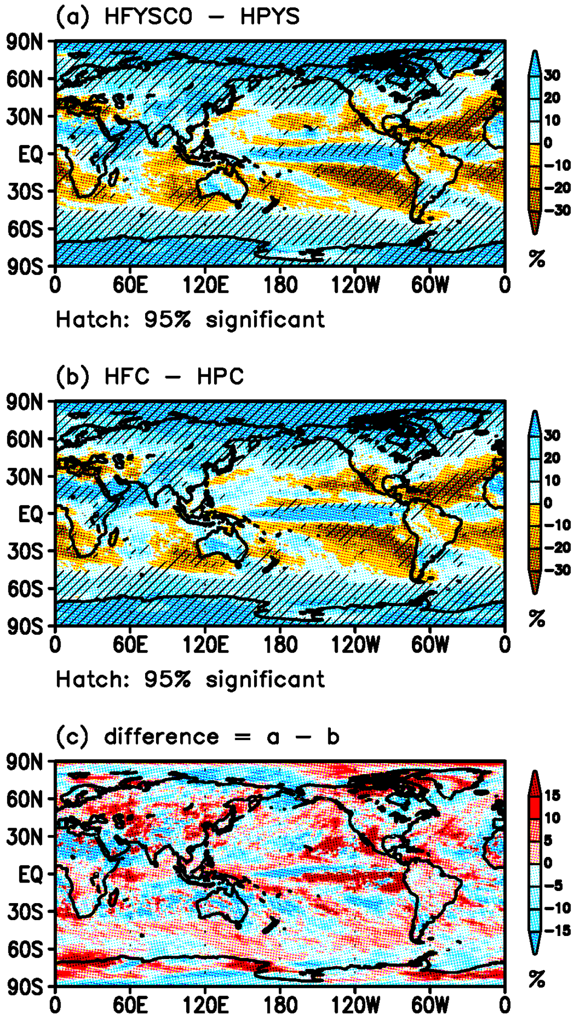

Figure S9. Comparison between future changes in annual average precipitation (PAV) by atmospheric model and AOGCM. (a) Future change by HFYSC0 (2079-2099, 21 years) - HPYS (1983-2003, 21 years). Change is normalized by HPYS. Hatched regions show changes above the 95% significance level. The 60-km model with the YS scheme is used. (b) Same as (a) but for AOGCM. The atmospheric part of AOGCM is the same as that used in (a). HPC: Present-day climate, HFC: Future climate. Heat flux adjustment is used to prevent large deviation from observed SST and future SST of CMIP5 AOGCMs. For detailed experimental design, see Ogata et al. (2015). (c) Difference defined as (a) minus (b).

ANalysis Of VAriance (ANOVA)

A two way of ANalysis Of VAriance (ANOVA; Storch and Zwiers 1999) is applied to future precipitation changes by the ensemble simulations of 60-km model with respect to three different cumulus convection schemes and four different sea surface temperature (SST) distributions. The total number of simulations amounts to 12 = 3 convections x 4 SSTs. The total variance among these simulations V is defined as

$$V = \sum_{i=1}^{I}\sum_{j=1}^{J}\left(x_{ij} - \overline{x}_{00}\right)^2,$$

where

x: precipitation change at a grid point

i: the kind of convection scheme

j: the kind of SST

I: the number of convection schemes, I=3

J: the number of SST, J=4

$$\overline{x}_{00} = \frac{1}{IJ}\sum_{i=1}^{I}\sum_{j=1}^{J} x_{ij}\,.$$

V can be decomposed into three terms such that

$$V = V_I + V_J + V_{IJ},$$

where

$$V_I = J\sum_{i=1}^{I}\left(\overline{x}_{i0} - \overline{x}_{00}\right)^2$$

$$V_J = I\sum_{j=1}^{J}\left(\overline{x}_{0j} - \overline{x}_{00}\right)^2$$

$$V_{IJ} = \sum_{i=1}^{I}\ \sum_{j=1}^{J}\left(x_{ij} - \overline{x}_{i0} - \overline{x}_{0j} + \overline{x}_{00}\right)^2$$

$$\overline{x}_{i0} = \frac{1}{J}\sum_{j=1}^{J} x_{ij}$$

$$\overline{x}_{0j} = \frac{1}{I}\sum_{i=1}^{I} x_{ij}\,.$$

The statistical significance of influence of convection (i) and SST (j) on the total variance V can be evaluated by the following quantities;

$$F_I = \frac{V_I / I_{m1}}{V_{IJ} / (I_{m1} J_{m1})}$$

$$F_J = \frac{V_J / J_{m1}}{V_{IJ} / (I_{m1} J_{m1})}$$

where

$I_{\mathrm{m1}} = I - 1$

$J_{\mathrm{m1}} = J - 1$.

F_I obeys the F distribution $F(I_{\mathrm{m1}}, I_{\mathrm{m1}} J_{\mathrm{m1}})$. F_J obeys the F distribution $F(J_{\mathrm{m1}}, I_{\mathrm{m1}} J_{\mathrm{m1}})$. Therefore, statistical significance can be evaluated for specified significance level.

Reference

Collins, M., R. Knutti, J. Arblaster, J.-L. Dufresne, T. Fichefet, P. Friedlingstein, X. Gao, W.J. Gutowski, T. Johns, G. Krinner, M. Shongwe, C. Tebaldi, A.J. Weaver and M. Wehner, 2013: Long-term Climate Change: Projections, Commitments and Irreversibility. In: *Climate Change 2013: The Physical Science Basis. Contribution of Working Group I to the Fifth Assessment Report of the Intergovernmental Panel on Climate Change* [Stocker, T.F., D. Qin, G.-K. Plattner, M. Tignor, S.K. Allen, J. Boschung, A. Nauels, Y. Xia, V. Bex and P.M. Midgley (eds.)]. Cambridge University Press, Cambridge, United Kingdom and New York, NY, USA.

Endo, H., A. Kitoh, T. Ose, R. Mizuta, and S. Kusunoki, 2012: Future changes and uncertainties in Asian precipitation simulated by multi-physics and multi-sea surface temperature ensemble experiments with high-resolution Meteorological Research Institute atmospheric general circulation models (MRI-AGCMs). *J. Geophys. Res*., **117**, D16118. doi:10.1029/2012JD017874

Endo, H., A. Kitoh, R. Mizuta, and M. Ishii, 2017: Future changes in precipitation extremes in East Asia and their uncertainty based on large ensemble simulations with a high resolution AGCM. *SOLA*, **13**, 7−12, doi:10.2151/sola.2017-002

Endo, H., A. Kitoh, R. Mizuta, and M. Ishii, 2017: Future changes in precipitation extremes in East Asia and their uncertainty based on large ensemble simulations with a high resolution AGCM. *SOLA*, **13**, 7−12, doi:10.2151/sola.2017-002.

IPCC (Intergovermental Panel on Climate Change), 2000: Special Report on Emissions Scenarios. A Special Report of Working Group III of the Intergovernmental Panel on Climate Change. [Nakic´enovic´, N., J. Alcamo, G. Davis, B. deVries, J.

Fenhann, S. Gaffin, K. Gregory, A. Grübler, T. Yong Jung, T. Kram, E.L. La Rovere, L. Michaelis, S. Mori, T. Morita, W. Pepper, H. Pitcher, L. Price, K. Riahi, A. Roehrl, H.-H. Rogner, A. Sankovski, M. Schlesinger, P. Shukla, S. Smith, R. Swart, S. van Rooijen, N. Victor, and Z. Dadi (eds.)]. Cambridge University Press, Cambridge, UK.

IPCC, 2013: *Climate change 2013: The physical science basis. Contribution of Working Group I to the Fifth Assessment Report of the Intergovernmental Panel on Climate Change.* Stocker, T.F.; Qin, D.; Plattner, G.K.; Tignor, M.; Allen, S.K.; Boschung, J.; Nauels, A.; Xia, Y.; Bex, V.; Midgley, P.M.; (ed) Cambridge University Press, Cambridge, United Kingdom and New York, NY, USA, 1535pp.

Kain, J. S. and J. M. Fritsch, 1990: A one-dimensional entraining/detraining plume model and its application in convective parameterization. J. Atmos. Sci., 47, 2784-2802. doi:10.1175/1520-0469(1990)047<2784:AODEPM>2.0.CO;2

Kitoh, A., and H. Endo, 2016: Changes in precipitation extremes projected by a 20-km mesh global atmospheric model. *Wea. Climate Extremes*, **11**, 41-52, doi.org/10.1016/j.wace.2015.09.001

Kitoh, A., and S. Kusunoki, 2007: East Asian summer monsoon simulation by a 20-km mesh AGCM. *Climate Dynamics*, **29**, doi:10.1007/s00382-007-0285-2

Kusunoki, S., 2016: Is the global atmospheric model MRI-AGCM3.2 better than the CMIP5 atmospheric models in simulating precipitation over East Asia? *Climate Dyn.*, doi:10.1007/s00382-016-3335-9

Kusunoki, S., 2017: Future changes in precipitation over East Asia projected by the global atmospheric model MRI-AGCM3.2. *Clim. Dyn.*, doi: 10.1007/s00382-016-3499-3

Kusunoki, S., and R. Mizuta, 2008: Future Changes in the Baiu Rain Band Projected by a 20-km Mesh Global Atmospheric Model: Sea Surface Temperature Dependence. *Scientific online Letters on the Atmosphere (SOLA)*, **4**, 85-88. doi:10.2151/sola 2008-022

Kusunoki, S. and R. Mizuta, 2012: Comparison of near future (2015-2039) changes in the East Asian rain band with future (2075-2099) changes projected by global atmospheric models with 20-km and 60-km grid size. *Scientific online Letters on the Atmosphere (SOLA)*, **8**, 73-76. doi:10.2151/sola.2012-019

Kusunoki, S., and R. Mizuta, 2013: Changes in precipitation intensity over East Asia during the 20th and 21st centuries simulated by a global atmospheric model with a 60 km grid size, *J. Geophys. Res. Atmos.*, 118, doi:10.1002/jgrd.50877

Kusunoki, S., J. Yoshimura, H. Yoshimura, A. Noda, K. Oouchi, and R. Mizuta, 2006: Change of Baiu rain band in global warming projection by an atmospheric general circulation model with a 20-km grid size. *J. Meteor. Soc. Japan*, **84**, 581-611. doi:10.2151/jmsj.84.581

Kusunoki, S., R. Mizuta and M. Matsueda, 2011: Future changes in the East Asian rain band projected by global atmospheric models with 20-km and 60-km grid size. *Climate Dynamics*, **37**, 2481-2493, doi:10.1007/s00382-011-1000-x

Kusunoki, S., R. Mizuta and M. Hosaka, 2015: Future changes in precipitation intensity over the Arctic projected by a global atmospheric model with a 60-km grid size. *Polar Science*, **9**, 277-292, doi:10.2467/mripapers.65.15

Mizuta, R., A. Murata, M. Ishii, H. Shiogama, K. Hibino, N. Mori, O. Arakawa, Y. Imada, K. Yoshida, T. Aoyagi, H. Kawase, M. Mori, Y. Okada, T. Shimura, T. Nagatomo, M. Ikeda, H. Endo, M. Nosaka, M. Arai, C. Takahashi, K. Tanaka, T.

Takemi, Y. Tachikawa, K. Temur, Y. Kamae, M. Watanabe, H. Sasaki, A. Kitoh, I. Takayabu, E. Nakakita, and M. Kimoto, 2016: Over 5000 years of ensemble future climate simulations by 60 km global and 20 km regional atmospheric models. *Bull. Amer. Meteor. Soc.*, doi:10.1175/BAMS-D-16-0099.1, Published Online: 30 November 2016

Ogata, T., R. Mizuta, Y. Adachi, H. Murakami, T. Ose, 2015: Effect of air-sea coupling on the frequency distribution of intense tropical cyclones over the northwestern Pacific. *Geophys. Res. Lett.*, **42**, 10,415–10,421, doi:10.1002/2015GL066774.

Randall, D., and D.-M. Pan, 1993: Implementation of theArakawa–Schubert cumulus parameterization with a prognostic closure. *The Representation of Cumulus Convection in Numerical Models, Meteor. Monogr.*, No. 46, Amer. Meteor. Soc., 137–144.

Storch, H.V. and F. W. Zwiers, 1999: Section 9 Analysis of variance. In *Statistical analysis in climate research*. Storch HV, Zwiers FW (eds), Cambridge University Press, Cambridge, pp 171–192

Yoshimura, H., Mizuta, R., Murakami, H., 2014: A spectral cumulus parameterization scheme interpolating between two convective updrafts with semi-Lagrangian calculation of transport by compensatory subsidence. *Mon. Wea. Rev.*, **143**, 597–621. doi:10.1175/MWR-D-14-00068.1